

High piezoelectric sensitivity and hydrostatic figures of merit in unidirectional porous ferroelectric ceramics fabricated by freeze casting

Yan Zhang, James Roscow, Mengying Xie, Chris Bowen

Department of Mechanical Engineering, University of Bath, BA2 7AY, United Kingdom

High performance lead zirconate titanate (PZT) ceramics with aligned porosity for sensing applications were fabricated by an ice-templating method. To demonstrate the enhanced properties of these materials and their potential for sensor and hydrophone applications, the piezoelectric voltage constants (g_{33} and g_{31}), hydrostatic parameters (d_h , g_h , $-d_{33}/d_{31}$, $d_h \cdot g_h$ and $d_h \cdot g_h/\tan\delta$) and AC conductivity as a function of the porosity in directions both parallel and perpendicular to the freezing temperature gradient were studied. As the porosity level was increased, PZT poled parallel to the freezing direction exhibited the highest d_h , $-d_{33}/d_{31}$ and figures of merit $d_h \cdot g_h$, $d_h \cdot g_h/\tan\delta$ compared to the dense and PZT poled perpendicular to the freezing direction. The g_h , g_{33} and g_{31} coefficients were highest for the PZT poled perpendicular to the freezing direction; the g_h was 150% to 850% times higher than dense PZT, and was attributed to the high piezoelectric activity and reduced permittivity in this orientation. This work demonstrates that piezoelectric ceramics produced with aligned pores by freeze casting are a promising candidate for a range of sensor applications and the polarisation orientation relative to the freezing direction can be used to tailor the microstructure and optimise sensitivity for sensor and hydrostatic transducer applications.

Introduction

Piezoelectric materials represent a popular class of active materials used in many areas[1-3], such as SONAR applications, vibration energy harvesting, structural health monitoring and non-destructive evaluation. For uniaxial sensing applications, the piezoelectric voltage constants g_{33} and g_{31} are important parameters since they represent the electric field produced per unit stress, and are of interest for accelerometers, force, pressure and acoustic sensors. Hydrophones that operate under hydrostatic conditions are also an important category of piezoelectric transducers, which are employed to detect acoustic signals in water by converting the mechanical vibrations of low frequency acoustic waves into an electrical signal[4]. For such applications, the important parameters are the hydrostatic charge (d_h) coefficient, voltage (g_h) coefficient, and hydrostatic figure of merit ($FoM_I=d_h \cdot g_h$), which define the actuating (transmit) capability of the material, sensitivity of the hydrophone, and the suitability for underwater sonar applications, respectively[5, 6]. At frequencies far below the resonance frequency,

energy dissipation is mainly dominated by the dielectric loss ($\tan \delta$), thus an alternative figure of merit of $FoM_2 = d_h \cdot g_h / \tan \delta$ has also been proposed [7, 8].

The hydrostatic figures of merit can be calculated from measured piezoelectric and dielectric properties as follows: $d_h = d_{33} + 2d_{31}$, $g_h = d_h / \epsilon_{33}^T \epsilon_0$, where, d_{33} and d_{31} are the longitudinal and transverse piezoelectric charge coefficients, ϵ_{33}^T is the relative permittivity at constant stress and ϵ_0 is the permittivity of the free space. These equations indicate that the important requirements for improved hydrostatic performance are a high hydrostatic charge coefficient (d_h) and low permittivity (ϵ_{33}^T). For many dense ferroelectric ceramic materials $d_{33} \approx -2d_{31}$ which leads to a low d_h , and when combined with the high permittivity of dense ferroelectrics this leads to dense materials exhibiting a low d_h , g_h , and $d_h \cdot g_h$, thereby limiting their performance as transducers under hydrostatic conditions. For uniaxial sensor applications, the combination of a high piezoelectric charge coefficient and low permittivity is also beneficial since $g_{33} = d_{33} / \epsilon_{33}^T \epsilon_0$ and $g_{31} = d_{31} / \epsilon_{33}^T \epsilon_0$.

To date, a number of researchers have made significant efforts to reduce the permittivity of the sensor material by introducing porosity into the dense material [9-12]. However, the compromise between the mechanical strength and the volume fraction and type of porosity remains a limiting issue, especially for those porous ceramics with randomly distributed porosity, which is typically achieved by a traditional processing route of adding a polymeric pore-forming agent that burns out during solid-state sintering. Furthermore, the production of aligned piezoelectric structures has recently attracted considerable interest due to their ability to reduce the resistance of piezoelectric domain motion under an applied electric field, where alignment has been explored using nanowires [13, 14], nanofibers [15], and nanopores [16].

In this paper, we exploit the inspiration drawn from the high strength of natural nacre with a layered microstructure [17], and the ability of freeze casting, also called ice-templating [18-20] as an effective way to mimic the structure of nacre by building an oriented ceramic structure within a unidirectional temperature gradient, with the realisation of anisotropic properties in directions parallel and perpendicular to the temperature gradient/pore channel. To date, there have been a number of studies on freeze-cast piezoelectric ceramics that have utilised camphene-based [21-23], tert-butyl alcohol (TBA)-based [24-34] suspensions to achieve 3-1, 3-2 and 3-3 connectivity piezoceramic-based composites, and water-based [34-40] suspensions for 2-2 connectivity composites. The majority of the investigations above were focused on the properties of the freeze-cast parallel to the temperature gradient/pore channel, and there is little work on comparing the piezoelectric properties of freeze-cast ceramics both parallel and perpendicular to the temperature gradient/pore channel.

TBA-based $0.94\text{Bi}_{0.5}\text{Na}_{0.5}\text{TiO}_3\text{-}0.06\text{BaTiO}_3$ [30] and $\text{K}_{0.5}\text{Na}_{0.5}\text{NbO}_3$ [31] suspensions were used to achieve an aligned porous ceramic by freeze casting, whose piezoelectric constants (d_{33} and g_{33}) and strain were examined, with differences between parallel and perpendicular orientations while the hydrostatic properties were evaluated in freeze casting camphene-based lead zirconate titanate-lead zinc niobate suspension [22]. However, camphene is potentially flammable and has been demonstrated

to exhibit higher toxicity than water [41], while TBA is not only a flammable, toxic and carcinogenic substance[42, 43], but is also an emerging environmental contaminant[44]. Moreover, laminated 2-2 connectivity based piezoelectric and pyroelectric composites are of interest due to their simple architecture and superior actuation and sensing abilities[45-47]. Therefore, using water as the solvent in the freeze casting process would be a more environmentally friendly choice with lower processing cost. In addition, our previous work[48, 49] has demonstrated that porous ceramics with an aligned porous structure formed by freeze casting water-based suspension exhibited an improved mechanical strength compared to traditional porous ceramic and also lead to a significantly reduced permittivity and heat capacity compared to that of the dense material. Since the aligned structure maintained high pyroelectric properties parallel to the freezing direction a higher charging voltage and energy was achieved when charging a capacitor via the pyroelectric effect for energy harvesting applications. However, apart from our previous research on energy harvesting applications [48], there have been no reports on the piezoelectric properties by freeze casting water-based piezoelectric suspensions and their assessment in both parallel and perpendicular directions for sensor and hydrostatic applications. Therefore, this paper provides a first insight into the properties of porous piezoelectric ceramic with aligned porosity by water based freeze casting for sensor and hydrostatic applications. The piezoelectric voltage constants (g_{33} and g_{31}), hydrostatic parameters (d_h , g_h , $-d_{33}/d_{31}$, $d_h \cdot g_h$ and $d_h \cdot g_h / \tan \delta$) and AC conductivity are assessed when the material was poled parallel and perpendicular directions to the freezing temperature gradient using a simple water-based suspension. Significant benefits will be demonstrated for many of the properties compared to the monolithic (dense) material, depending on the polarisation direction.

Methods

The raw materials used for water-based freeze casting process to fabricate the aligned porous PZT were reported in our previous work on energy harvesting[48]. Figure 1 shows images of the PZT powders before and after ball milling used in this work. It can be seen that the original as-received PZT powders exhibited a sphere-like morphology due to the spray drying processing, whose agglomerate particle diameter was approximately 40 μm , as shown in Fig. 1(A). According to our previous research[50, 51], the ceramic particle size has a strong influence on the rheological properties of the suspension, which is crucial not only for the stability of the suspension for pore preparation by freeze casting, but also the pore size of the porous channel and the final properties. Normally, the particle size of the ceramic[52] in the suspension should range from submicron to less than 3 μm in order to exhibit suitable stability and viscosity for freeze casting[53-56]. Therefore, in order to improve the rheological properties of the suspension for achieving the defect-free ceramic layer by freeze casting, a high-speed ball milling treatment in ethanol was utilised, and the particle

size of the PZT powders with uniform shape were reduced to approximately 1 μm on average in Fig. 1(B).

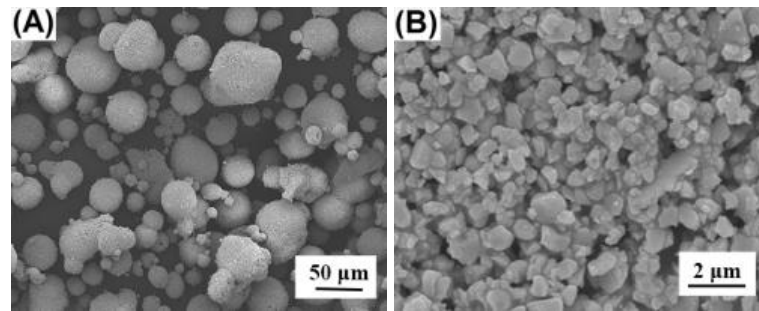


Figure 1 SEM images of PZT powders (A) without ball milling ('as-received'), (B) after ball milling for 48h.

A schematic of the freeze casting process is shown in Fig. 2. The PZT suspensions with the solid load levels of 67, 58, 48.5, 35.5, 22.5 vol.% were ball-milled for 24 h in zirconia media to generate homogeneous and fine suspensions. The prepared suspensions were de-aired (Fig. 2 (A)) before casting into a cylindrical polydimethylsiloxane (PDMS) mould with four cylinder shaped chambers (shown in Fig. S1) which was transported to a conducting cold plate in a liquid nitrogen container for the freeze casting process (Fig. 2 (B)); in this figure the freezing direction is from the base and upwards which leads to the structure shown in the image. After freezing, the frozen bodies were demoulded and freeze-dried in a vacuum at $-50\text{ }^{\circ}\text{C}$ to sublimate the ice crystal (Fig. 2 (C)) to form a 2-2-type connectivity with the PZT material aligned in the freezing direction, but more randomly orientated perpendicular to the freezing direction. To compare with the freeze cast ceramics, dense PZT pellets were formed with the initial diameter of 10 mm and thickness of 1.2 mm by uniaxial hydraulic pressing. Finally, the porous (freeze cast) and dense (pressed) green bodies were sintered at $1250\text{ }^{\circ}\text{C}$ for 2 h under a PbO-rich after organic additives burnt out at $600\text{ }^{\circ}\text{C}$ for 3 h. Each porous PZT cylinder was poled parallel and perpendicular to the freezing direction, denoted as PZT_{\parallel} and PZT_{\perp} , respectively for the following microstructure and assessment of piezoelectric properties. A schematic showing the freezing, cutting, poling directions and SEM viewing orientation are also summarised in Fig. S2.

The microstructures of the powders and sliced PZT ceramics were examined by a scanning electron microscopy (SEM, JSM6480LV, Tokyo, Japan). The apparent porosity was derived from the density data obtained by the Archimedes method with the error of $\pm 1.5\text{ vol.}\%$. Each porosity was labelled with the integer value. The remnant polarization and coercive field of the ceramics were measured using a Radiant RT66B-HVi Ferroelectric Test System on initially unpoled materials. The longitudinal piezoelectric strain coefficient (d_{33}) and the transverse piezoelectric strain coefficient (d_{31}) were measured using a Berlincourt Piezometer (PM25, Take Control, UK) after corona poling by applying a DC voltage of 14 kV for 15 min at $120\text{ }^{\circ}\text{C}$. The AC conductivity, σ , of the sintered

ceramics were carried out from 0.1Hz to 1MHz at room temperature using an impedance analyzer (Solartron 1260, Hampshire, UK) and calculated from equation (1)[57],

$$\sigma = \frac{Z'}{Z'^2 + Z''^2} \cdot \frac{t}{A} \quad (1)$$

where Z' and Z'' are the real and imaginary parts of the impedance, A is the area of the sample and t is the sample thickness.

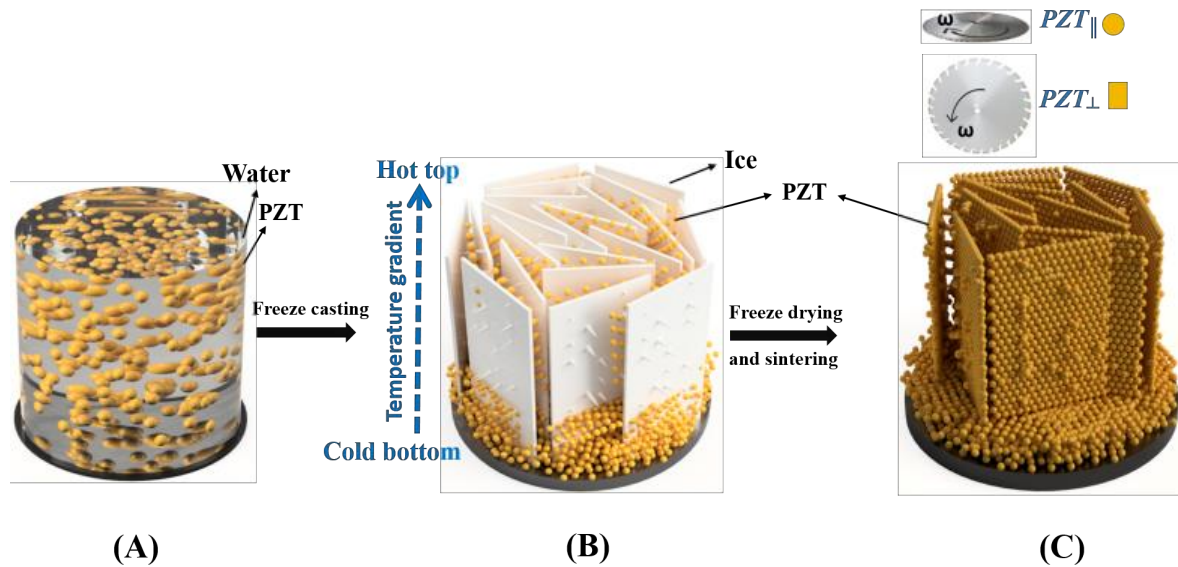


Figure 2 Schematic of porous PZT preparation by freeze casting. (A) water-based PZT suspension in each cylindrical chamber of the mould, (B) freezing of the water from the cold base, (C) freeze drying leading to a layered PZT structure.

The freezing direction is indicated (form bottom to top) along with the polarisation direction for samples poled along freezing direction (PZT_{\parallel}) and perpendicular to freezing direction (PZT_{\perp}).

Results and discussion

Figure 3(A) and (B) show SEM micrographs of the porous PZT poled parallel and perpendicular to the freezing direction, respectively. A dense lamellar ceramic wall can be seen in Fig. S3, which is desirable for high piezoelectric activity. From the macro-scale point of view, the microstructure on the top face as shown in Fig. 3(A) is equivalent to looking from above of Fig. 1(C), compared to the side face in Fig. 3(B) which is equivalent to looking from the side of Fig. 1(C). Due to the random nature of ice nucleation in the single vertical temperature gradient condition [58], there were multiple orientations on the top face of PZT_{\parallel} as shown in the Fig. 3(A), while clear alignment of the PZT material with good parallelism of the lamellar ceramic layer can be readily observed in PZT_{\perp} , although part of the lamellar layers were covered by their adjacent layers in the PZT_{\perp} , as shown in the Fig. 3(B).

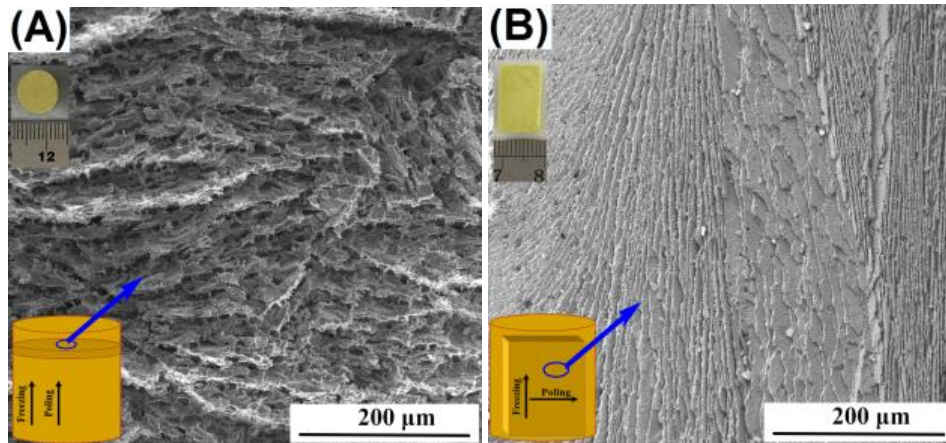
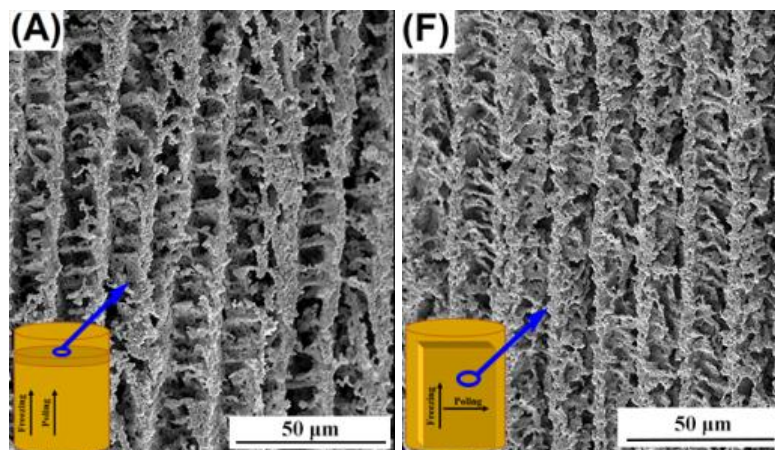
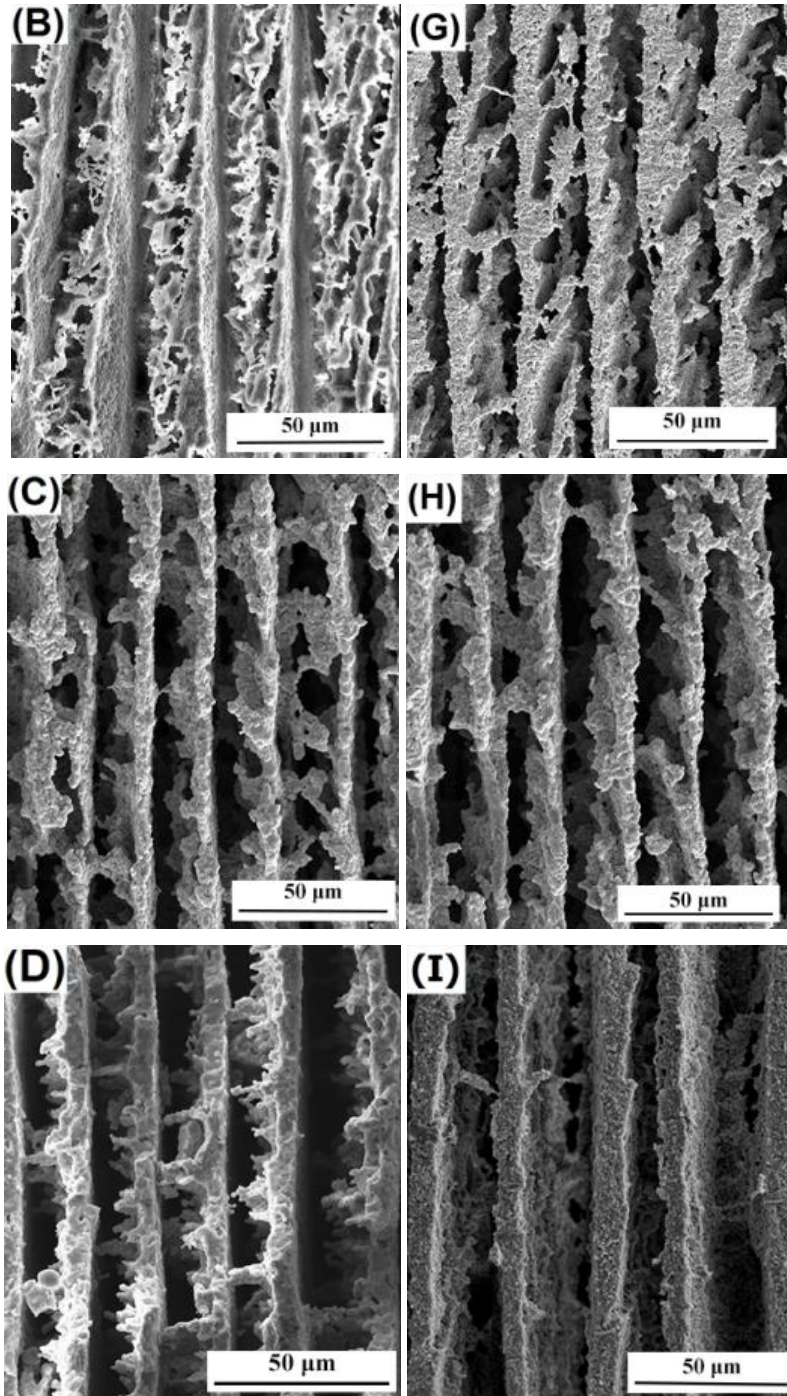


Figure 3 SEM micrographs of porous (A) $PZT_{||}$ and (B) PZT_{\perp} .

Figure 4 (A-E) and (F-J) show SEM micrographs of the microstructure parallel ($PZT_{||}$) and perpendicular (PZT_{\perp}) to the freezing direction as the porosity fraction is increased from 20-60 vol.%, respectively. The specific porosities of 20-60 vol.% were achieved based on the results from the initial experiments that employed a ranges of solid load levels, shown in Fig. S4. With an increase of porosity, the lamellar pore size decreased while the number of the dendrites decreased accordingly in both the $PZT_{||}$ and PZT_{\perp} materials. In the 20 vol.% PZT, a large quantity of the dendrites on the lamellar surface can be found, and most of the dendrites were connected with the adjacent ceramic layer, as shown in Fig. 4 (A) and (F). These additional dendrites are beneficial not only for piezoelectric phase connection, but also for the improvement of mechanical strength. It can be seen that when the porosity reached 60 vol.%, the surface of the lamellar layers became relatively smooth with ceramic links on the edge of the layers, as shown in Fig. 4(E) and (J). In the freeze casting process, a low freezing rate can provide a longer period for ice growth, which is the replica of the lamellar pore in the SEM images, while a low solid loading can provide a low viscosity which facilitates ceramic particle rearrangement. Both of the above conditions can lead to a large lamellar pore size and the high porosity materials exhibiting a smaller number of dendrites.





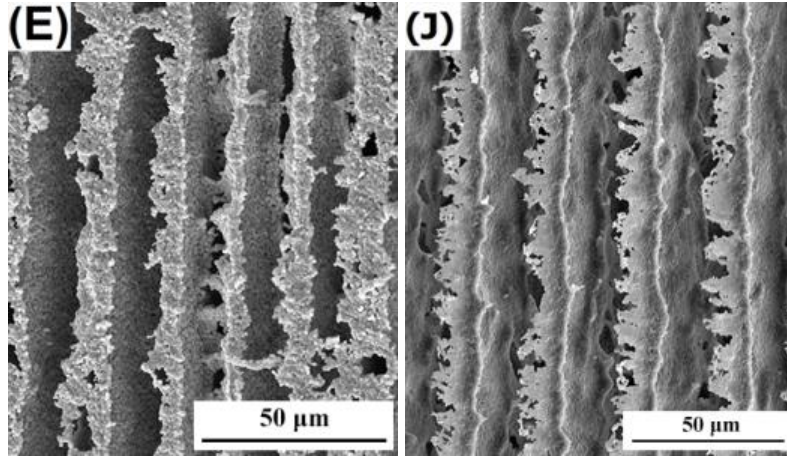


Figure 4 SEM images of porous $PZT_{||}$ with the porosity of (A) 20, (B) 30, (C) 40, (D) 50, and (E) 60 vol.% and PZT_{\perp} with the porosity of (F) 20, (G) 30, (H) 40, (I) 50, and (J) 60 vol.%.

Figure 5 shows the remnant polarisation (P_r) and coercive field (E_c) of the initially unpoled porous PZT as a function of the porosity ranging from 20 to 60 vol.%, respectively. It can be observed that the P_r of both $PZT_{||}$ and PZT_{\perp} decreased with an increase of porosity, which were 2.1-5.5 and 3.1-10.0 times lower than the dense PZT, respectively. The dense material is characterised as having 4 vol.% porosity, with the density of 7.2 g/cm^3 based on the theoretical density of 7.5 g/cm^3 from the datasheet provided by the supplier. The reduction in P_r is likely to be due to the reduced amount of polarised material and the inhomogeneous electric field distribution in the porous materials as a result of the contrast in permittivity between the high-permittivity PZT and low-permittivity air. The decrease of P_r is also associated with its connectivity (Fig. 3A), and leads to a decrease of piezoelectric properties[48], such as d_{33} and d_{31} . The decrease in P_r with porosity is more rapid than predicted by $P_r^{porous} = P_r^{dense} \times (1-p)$ where p is porosity [59]; this is due to the porosity also restricting polarisation of the ceramic since the electric field concentrates in the lower permittivity pore space. The $PZT_{||}$ material exhibited a 1.5-1.8 times higher P_r compared to the PZT_{\perp} due to the improved connectivity of piezo-active material along the freezing direction and therefore the lower fraction of unpoled areas in $PZT_{||}$ [48, 60]. The E_c values of both $PZT_{||}$ and PZT_{\perp} increased as the porosity increased, see Fig. 5B, and the PZT_{\perp} exhibited the highest E_c values in all ranges of porosity. The increase in E_c with porosity is due to the concentration of the applied electric field in the low permittivity pore space, leading to higher applied electric field being required to achieve domain switching in the higher permittivity ferroelectric phase. For the same reason, a higher E_c is observed for the PZT_{\perp} material as there is a reduced connection of ferroelectric along this poling direction as a result of the overlapped lamellar layers, see Fig. 3(D), resulting in a reduced piezoelectric response[61] and a higher E_c in PZT_{\perp} . The inhomogeneous electric field due to the presence of pores is also reflected in the reduced rectangularity ($P_{remnant}/P_{saturation}$) of the materials as the porosity level increases, as seen in Fig. 5(C).

Interestingly, the PZT_{\parallel} with the porosity of 20 vol.% exhibited the lowest E_c of 7.7 kV/cm compared to both the dense (8.7 kV/cm), and all the PZT_{\perp} materials, demonstrating easier switching of ferroelectric domains with applied electric field. The presence of a small amount of porosity (~20 vol.%) may initially provide a state of reduced internal stress or restriction of domain motion, while at higher porosity levels the applied electric field concentrates in the pore volume and leads to higher applied electric fields being required to provide domain switching. Therefore, although the existence of porosity can facilitate the switching of the domain walls to some extent[62, 63], the increased electric field concentration[60] in the low permittivity pore space leads to a higher E_c which reached to $8.9 \mu\text{C}/\text{cm}^2$ compared to the dense with the E_c of $8.7 \mu\text{C}/\text{cm}^2$ when the porosity was higher than 50 vol.%.

In addition, due to randomness of the lamellar pores orientations perpendicular to the freezing direction in Fig. 3 (A) and Fig. 2 (C), the angle of the pore in PZT_{\perp} ranged from $>0^\circ$ to 90° , while PZT_{\parallel} had an angle of $\sim 0^\circ$ along the poling direction; see Fig. S5. This leads to a better level of poling of PZT_{\parallel} [64] compared to PZT_{\perp} , leading to a higher polarisation for PZT_{\parallel} [48, 64], as seen in Fig. 5(A).

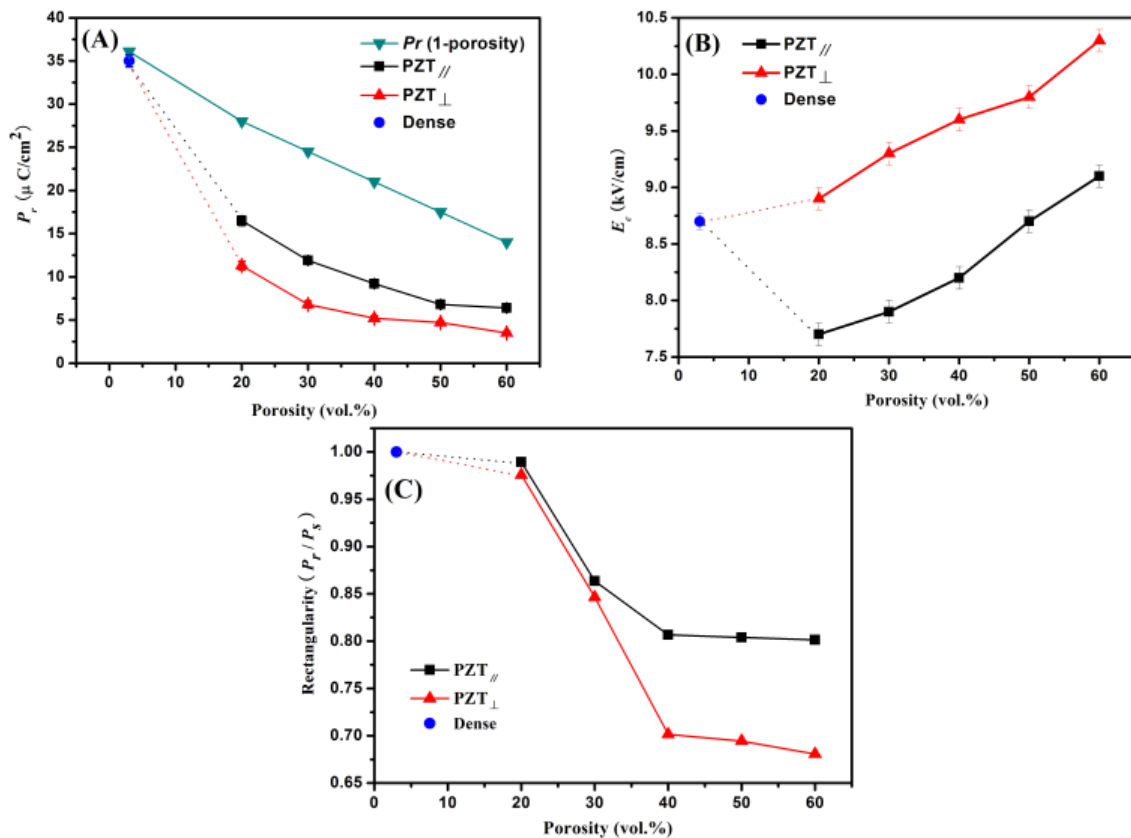


Figure 5 (A) Remnant polarisation (P_r), along with estimation based on $P_r^{porous} = P_r^{dense} \times (1-p)$, (B) coercive field (E_c) of the porous freeze-cast PZT, and (C) rectangularity ratio of with P_r/P_s various porosities. The dense material is also shown.

Figure 6 (A-F) show the anisotropy factor[65] $-d_{33}/d_{31}$, hydrostatic charge (d_h), voltage coefficient (g_h), piezoelectric voltage coefficients (g_{33} and g_{31}), relative permittivity (ϵ_{33}^T) and figures of merit ($d_h g_h$ and $d_h g_h / \tan \delta$) of the porous PZT as a function of the porosity ranging from 20 to 60 vol.% and dense PZTs. It can be seen from Fig. 6(A) that PZT_{\perp} exhibited a lower $-d_{33}/d_{31}$ than the dense PZT at all porosities, while porous PZT_{\parallel} exhibited a higher $-d_{33}/d_{31}$ and therefore higher anisotropy than the dense PZT. The $-d_{33}/d_{31}$ PZT_{\parallel} increased with increasing porosity and was 1.2-2.0 times higher than that of PZT_{\perp} . The increase in piezoelectric anisotropy for PZT_{\parallel} is advantageous since it leads to higher d_h values that were determined from the d_{33} and d_{31} , as shown in Fig. 6(B). It can be seen the PZT_{\perp} exhibits a gradual reduction in d_h with increasing porosity, due to a reduced $-d_{33}/d_{31}$ while the PZT_{\parallel} exhibits an increase in d_h with increasing porosity. It should be also noted in Fig. 6(B) that the d_h of the PZT_{\parallel} was higher than the dense PZT when the porosity exceeded 40 vol.%. The increase in d_h for the porous material compared to the dense material is relatively modest, this is due to the fact that the dense material already has a relatively high degree of anisotropy with a $-d_{33}/d_{31}$ of ~ 3 (see Figure 6A); typically $-d_{33}/d_{31}$ is close to 2 for dense PZT based materials.

While the PZT_{\perp} materials exhibited relatively poor d_h values it exhibits advantageous g_h values that are 1.2 to 2.1 times and 1.5-8.5 higher than PZT_{\parallel} and monolithic dense PZT, respectively; see Fig. 6(B), i.e. 40.1×10^{-3} Vm/N for PZT_{\parallel} , and 83.5×10^{-3} Vm/N for PZT_{\perp} both at 60 vol.% porosity compared to that of dense PZT (9.0×10^{-3} Vm/N). This was due to the reduced relative permittivity, shown in Fig. 6(C) and (D), of the PZT_{\perp} ($\epsilon_{33}^T \sim 380$ to 16) compared to PZT_{\parallel} ($\epsilon_{33}^T \sim 1407$ to 581) and the dense material ($\epsilon_{33}^T = 2158$); at 1 kHz from the inset of Fig. 6(C) and (D). The g_h value of the PZT_{\parallel} was also 1.3-4.1 times higher than that of the dense PZT (see Fig. 6(B)) since the dense material exhibited a much higher permittivity, Fig. 6(C).

A similar trend is observed on examination of the piezoelectric voltage coefficients (g_{33} and g_{31}) in Fig. 6 (E) where both g_{33} and g_{31} of PZT_{\perp} were 1.8-5.2 and 2.0-10.0 times higher than PZT_{\parallel} , and also 2.3-12.5 and 2.5-14.7 times higher than dense PZT. This indicates that PZT_{\perp} is attractive as a piezoelectric force/pressure sensor. Fig. 6(F) shows that both the $d_h \cdot g_h$ and $d_h \cdot g_h / \tan \delta$ figures of merit for the PZT_{\parallel} increased with increasing porosity, and were much larger than both the dense material and PZT_{\perp} . Although a reduced inter-connection of the piezoelectric phase was observed with an increase of porosity (see Fig. 4), the high degree of alignment of the pore channel along the poling direction can compensate for the reduction in interconnectivity, especially in PZT_{\parallel} . This is due to a combination of, relatively high piezoelectric activity (Fig. 5), high piezoelectric coefficients, high anisotropy and low permittivity achieved through the introduction of the porosity. These results compare favourably with previous analysis[48] that demonstrated the higher $d_{33} \cdot g_{33}$ piezoelectric and pyroelectric harvesting figures of merit ($(\text{pyroelectric coefficient})^2 / \text{permittivity} \cdot \text{heat capacity}$) in PZT_{\parallel} .

The highest values of hydrostatic figures of merit were achieved for PZT_{\parallel} when the porosity increased to the maximum value of 60 vol.% in this work; this corresponded to hydrostatic figures of merit that

were 2.7-10.2 and 2.0-10.9 times higher than the dense materials and PZT_{\perp} , respectively, as shown in Fig. 6(D). The 60 vol.% was chosen as a maximum since for higher porosity levels the material will exhibit reduced mechanical properties, and an even higher coercive field; leading to a low d_{33} and therefore a low d_h . In addition to the advantages of high mechanical strength reported previously[48, 49], the freeze-cast samples exhibited comparable or even higher hydrostatic figure-of-merit than most of other processing methods, especially PZT_{\parallel} which exhibit a higher piezoelectric coefficient and lower permittivity, as shown in Table 1. It can be seen that freeze casting generally leads to high hydrostatic figures of merit compared to other methods. Very high figures of merit are reported in Table 1 for PZT-lead zirconate niobate (PZN) [22], which is due to the high porosity levels (90vol.%); although mechanical properties can be a concern at such low ceramic volume fractions.

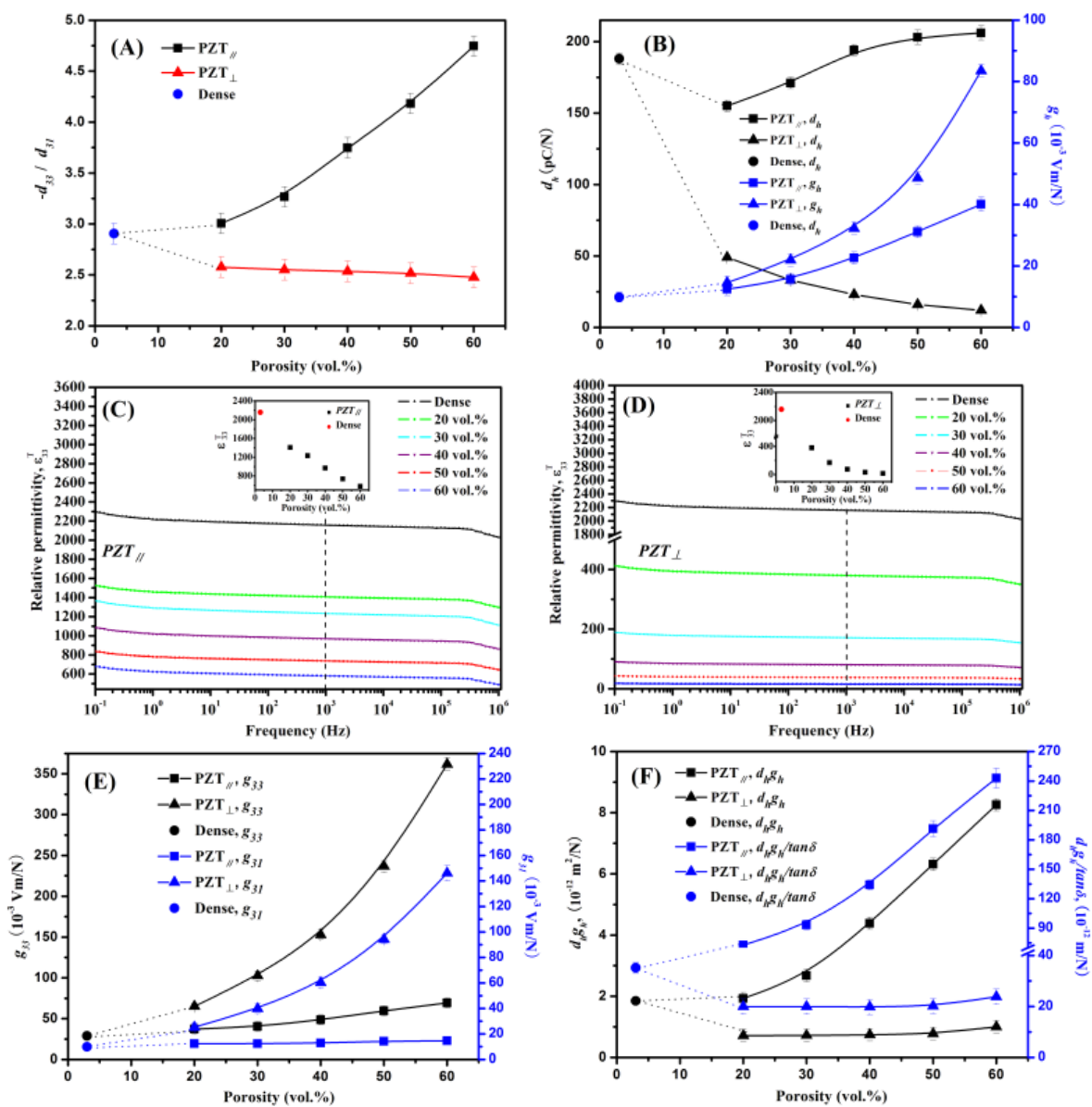


Figure 6 (A) anisotropy factor of $-d_{33}/d_{31}$, (B) hydrostatic charge (d_h) and voltage coefficient (g_h), (C) (D) relative permittivity (ϵ_{33}^T), (E) piezoelectric voltage coefficients (g_{33} and g_{31}), and (F) hydrostatic figure of merits ($d_h g_h$ and $d_h g_h / \tan \delta$) of the porous freeze-cast PZT with various porosities. The dense material is also shown.

Table 1 Comparison of hydrostatic parameters with different processing methods for lead zirconate titanate (PZT) or PZT-based composite. PZN = lead zirconate niobate.

Production method	Composite		Connectivity	PZT Volume %	d_h (pC/N)	g_h (10^{-3} Vm/N)	$d_h g_h$ (10^{-12} m ² /N)	Ref.
Freeze casting	PZT-air (water-based)	Parallel	2-2	40	206	40.1	8.26	This work
		Perpendicular			12	83.5	1	
	PZT/PZN-air (camphene-based)	Parallel	3-3	~10	406	396	161.01	[22]
		Pore orientation of 45° to poling direction			~350	~330	~115.5	
		Perpendicular			216	241	53.13	
	PZT/PZN-air (camphene-based)	Parallel	3-3	~48	~250	~32	~8	[23]
	PZT-air (TBA-based)	Parallel	1-3	31.3	-	-	9.32	[25]
	PZT-air (TBA-based)	Parallel	3-3	~60	-	-	7.6	[33]
	PZT-air (TBA-based)	Parallel	3-3	41.4	200	-	10.11	[32]
PZT-air (alginate/water-based)	Parallel	3-1	43.22	~223	-	~5.7	[37]	
BURPS (Burnout of Polymer Spheres)	PZT-air		3-0	54.5	~35	~16.4	~0.57	[66]
			3-1	59	-	~42	~5	[67]
			3-3	~60	102	72	7.3	[10]
			3-0	68	-	~48	5	[68]
Ionotropic gelation process	PZT-air		3-1	~44	~222	-	~5.6	[37]
Pore-forming agent	PZT-epoxy		3-1	45-60	60	69	~4.01	[69]
Polymer injection (PZT rods embedded in polymer)	PZT-polymer		1-3	40	~95	~18	~1.71	[70, 71]
Direct-write	PZT-polymer		2-2	~30	<190	<0.38	<0.72	[72]
Dice-and-fill	PZT-polymer		1-3	40	~135	~37	~5	[73]
	PZT-cement		2-2	40	<100	<0.2	<0.02	[74]

Figure 7 (A) and (B) show the AC conductivity (σ) of the PZT_{\parallel} and PZT_{\perp} at frequencies ranging from 0.1 to 10^6 Hz at room temperature respectively. It is clear from these two figures that the AC conductivity decreased with an increase of the porosity in both PZTs and were lower than that of the dense PZT at all the porosities and the frequencies; this includes the lowest frequencies where the conductivity is becoming less frequency dependent and is approaching the DC conductivity. The PZT_{\parallel} possessed a higher AC conductivity than the PZT_{\perp} at the same porosity and frequency, e.g. 1.3-

1.5 times at the frequency of 1 kHz, as shown in the insets in Fig. 7 (A) and (B). This is likely to be due to the high permittivity of the PZT_{\parallel} resulting from the contribution of the dielectric phase to the overall conductivity ($\omega\epsilon_r\epsilon_0$)[75]. Generally, there are two well-known models for interpreting the effects of porosity on electrical conductivity, where the solid phase has a small, but finite conductivity, and the pores have a very small (almost negligible) conductivity. For a composite consisting of both PZT and air, the low frequency conductivity parallel to the poling direction σ_{\parallel} (parallel connected) and PZT perpendicular to the freezing direction (series-connected) σ_{\perp} , which can be calculated as $\sigma_{\parallel} = v_{PZT}\sigma_{pzt} + v_{air}\sigma_{air}$ and $\sigma_{\perp} = \frac{\sigma_{PZT}\sigma_{air}}{V_{air}\sigma_{PZT} + V_{PZT}\sigma_{air}}$, where v_{PZT} and v_{air} are the volume fractions of PZT and air, σ_{pzt} and σ_{air} are the electric conductivity of the dense PZT and air[76]. Although $\sigma_{pzt} \gg \sigma_{air}$, no linear relation was found between conductivity σ and the porosity, as shown in the insets in Fig. 7 (A) and (B), owing to the existence of the dendritic ceramic link between the adjacent ceramic layers shown in Fig. 4, which means the pore regions were a mixture of the PZT ceramic links and the air. Similar situations can be also found in the piezoelectric and pyroelectric properties[48]. Furthermore, along the electric field direction during the impedance measurement, much more effective interface areas between the active phase PZT and the passive phase air were formed in the porous PZT_{\parallel} , therefore, the better ability of the domain movement and carrier mobility were the main reasons for the higher conductivity in the porous PZT_{\parallel} , making it be a more suitable candidate for hydrostatic sensor applications.

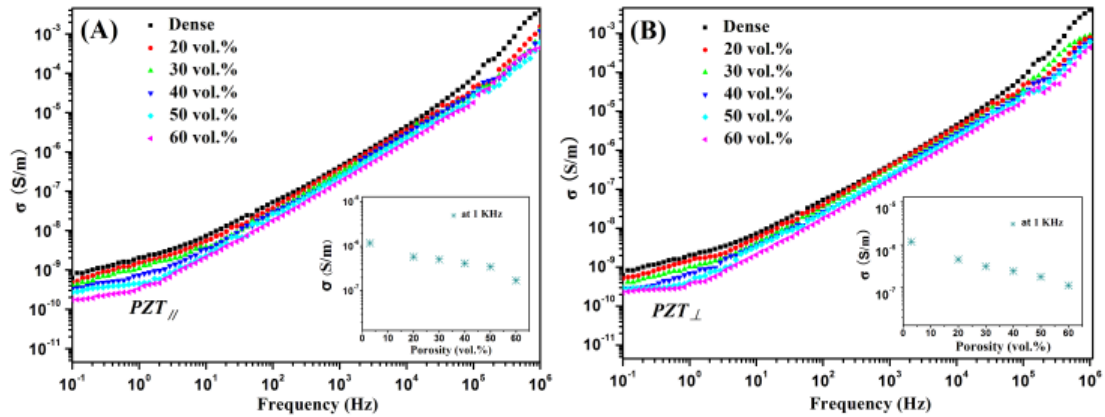


Figure 7 AC conductivity (σ) of the (A) PZT_{\parallel} and (B) PZT_{\perp} with various porosities. Insets in (A) and (B) are σ values of the PZT_{\parallel} and PZT_{\perp} at 1 kHz as a function of porosity, respectively. The dense material is also shown.

Conclusions

Freeze casting using a water based suspension has been utilised and demonstrated to be an effective method to prepare high performance porous PZT for sensor applications with unidirectional pore channels over a range of 20-60 vol. % porosity. The hydrostatic and sensor properties of PZTs poled parallel (PZT_{\parallel}) and perpendicular (PZT_{\perp}) to the freezing direction were examined in detail.

Significant improvements in the hydrostatic figures of merit were observed compared to the dense monolithic material. In terms of $d_h \cdot g_h$ and $d_h \cdot g_h / \tan \delta$, the PZT_{\parallel} and PZT_{\perp} were 2.7-10.2 and 2.0-10.9 times higher than that of the dense material. These highly attractive properties are due to their relatively high d_{33} , reduced d_{31} and significantly reduced permittivity. While the PZT_{\parallel} exhibited the best d_h , $d_h \cdot g_h$ and $d_h \cdot g_h / \tan \delta$, the PZT_{\perp} exhibited the highest g_h , g_{33} and g_{31} coefficients which was attributed to the lower permittivity of the material in this orientation. In addition, the PZT_{\parallel} showed 1.3-1.5 times higher AC conductivity than the PZT_{\perp} at the frequency of 1 kHz. In addition, it is shown that the properties are improved compared to piezoelectric composite materials manufactured by more complex methods. The PZT_{\perp} exhibited the highest g_h , g_{33} and g_{31} coefficients; up to 1.5-8.5, 2.3-12.5 and 2.5-14.7 times higher compared to the dense materials; this was attributed to the low permittivity of the material in this orientation. The coercive field increased with an increase in porosity for the materials, and this was attributed to the concentration of electric field concentration in the lower permittivity pore space. This work demonstrates water-based freeze casting provides an environmentally friendly and promising route to fabrication porous piezoelectric for both uniaxial and hydrostatic sensing applications with potential for control of the coercive field of ferroelectric materials. It is also demonstrated that changing of the poling condition relative to the freezing direction can enable control and optimisation of the relevant performance figures of merit for specific applications. In addition to varying the solid load levels, the ability of the freeze casting method to adjust the pore size, the thickness of the ceramic wall and the density of the ceramic wall in the aligned pore structures by tailoring the freezing rate, freezing temperature and temperature gradient provides significant versatility for this promising processing route to create new sensor materials.

Acknowledgment

Dr. Y. Zhang would like to acknowledge the European Union's Horizon 2020 research and innovation programme under the Marie Skłodowska-Curie Grant, Agreement No. 703950 (H2020-MSCA-IF-2015-EF-703950-HEAPPs). Prof. C. R. Bowen, Dr. M. Xie and Mr J. Roscow would like to acknowledge the funding from the European Research Council under the European Union's Seventh Framework Programme (FP/2007–2013)/ERC Grant Agreement No. 320963 on Novel Energy Materials, Engineering Science and Integrated Systems (NEMESIS).

References

- [1] R. Xie, X. Wang, G. Peng, T. Xie, D. Zhang, K. Zhou, G. Huang, G. Wang, H. Wang, A modified gelcasting approach to fabricate microscale randomized 1–3 piezoelectric arrays, *Ceramics International* 43(1) (2017) 144-148.
- [2] C.R. Bowen, M. Lopez-Prieto, S. Mahon, F. Lowrie, Impedance spectroscopy of piezoelectric actuators, *Scripta Materialia* 42(8) (2000) 813-818.

- [3] C.R. Bowen, A. Perry, A.C.F. Lewis, H. Kara, Processing and properties of porous piezoelectric materials with high hydrostatic figures of merit, *Journal of the European Ceramic Society* 24(2) (2004) 541-545.
- [4] R.Y. Ting, A review on the development of piezoelectric composites for underwater acoustic transducer applications, *Conference Record. IEEE Instrumentation and Measurement Technology Conference*, 1991, pp. 410-413.
- [5] H. Kara, R. Ramesh, R. Stevens, C.R. Bowen, Porous PZT ceramics for receiving transducers, *IEEE Transactions on Ultrasonics, Ferroelectrics, and Frequency Control* 50(3) (2003) 289-296.
- [6] A. Safari, Y.H. Lee, A. Halliyal, N.R. E., 0-3 piezoelectric composites prepared by coprecipitated PbTiO_3 powder, *American Ceramic Society Bulletin* 66 (1987) 668-670.
- [7] H. Li, D. Deng, Carlson Thomas J, Piezoelectric materials used in underwater acoustic transducers, *Sensor Letters* 10(3-4) (2012) 679-697.
- [8] P. S., Criterion for material selection in design of bulk piezoelectric energy harvesters, *IEEE Transactions on Ultrasonics, Ferroelectrics and Frequency Control* 57(12) (2010) 2610-2012.
- [9] I. Katsuyoshi, M. Toshimasa, O. Seiji, N. Kunihiro, Hydrophone sensitivity of porous $\text{Pb}(\text{Zr}, \text{Ti})\text{O}_3$ ceramics, *Japanese Journal of Applied Physics* 33(9S) (1994) 5381.
- [10] Y.-C. Chen, S. Wu, Piezoelectric composites with 3-3 connectivity by injecting polymer for hydrostatic sensors, *Ceramics International* 30(1) (2004) 69-74.
- [11] C.N. Della, D. Shu, The performance of 1–3 piezoelectric composites with a porous non-piezoelectric matrix, *Acta Materialia* 56(4) (2008) 754-761.
- [12] W.R. McCall, K. Kim, C. Heath, G. La Pierre, D.J. Sirbuly, Piezoelectric Nanoparticle–Polymer Composite Foams, *ACS Applied Materials & Interfaces* 6(22) (2014) 19504-19509.
- [13] C. Ou, P.E. Sanchez-Jimenez, A. Datta, F.L. Boughey, R.A. Whiter, S.-L. Sahonta, S. Kar-Narayan, Template-assisted hydrothermal growth of aligned zinc oxide nanowires for piezoelectric energy harvesting applications, *ACS Applied Materials & Interfaces* 8(22) (2016) 13678-13683.
- [14] Z. Zhou, H. Tang, H.A. Sodano, Vertically Aligned Arrays of BaTiO_3 Nanowires, *ACS Applied Materials & Interfaces* 5(22) (2013) 11894-11899.
- [15] J. Yan, Y.G. Jeong, High performance flexible piezoelectric nanogenerators based on BaTiO_3 nanofibers in different alignment modes, *ACS Applied Materials & Interfaces* 8(24) (2016) 15700-15709.
- [16] A. Castro, P. Ferreira, P.M. Vilarinho, Block copolymer-assisted nanopatterning of porous lead titanate thin films for advanced electronics, *The Journal of Physical Chemistry C* 120(20) (2016) 10961-10967.
- [17] A. P. Jackson, J. F. V. Vincent, R. M. Turner, The Mechanical Design of Nacre, *Proceedings of the Royal Society of London. Series B. Biological Sciences* 234(1277) (1988) 415-440.

- [18] S. Flauder, R. Sajzew, F.A. Müller, Mechanical properties of porous β -Tricalcium phosphate composites prepared by ice-templating and poly(ϵ -caprolactone) impregnation, *ACS Applied Materials & Interfaces* 7(1) (2015) 845-851.
- [19] F. Bouville, E. Portuguesez, Y. Chang, G.L. Messing, A.J. Stevenson, E. Maire, L. Courtois, S. Deville, Templated Grain Growth in Macroporous Materials, *Journal of the American Ceramic Society* 97(6) (2014) 1736-1742.
- [20] C. Stolze, T. Janoschka, S. Flauder, F.A. Müller, M.D. Hager, U.S. Schubert, Investigation of Ice-Templated Porous Electrodes for Application in Organic Batteries, *ACS Applied Materials & Interfaces* 8(36) (2016) 23614-23623.
- [21] M.-J.P. E.P.Gorzowski, and B. A. Bender, Prototype capacitor produced by freeze tape-casting, *International Symposium on Applications of Ferroelectrics*, July 2011, pp.1-3, 2011.
- [22] S.H. Lee, S.H. Jun, H.E. Kim, Y.H. Koh, Piezoelectric properties of PZT-based ceramic with highly aligned pores, *Journal of the American Ceramic Society* 91(6) (2008) 1912-1915.
- [23] S.-H.J. S.-H. Lee, H.-E. Kim, Y.-H. Koh, Fabrication of porous PZT–PZN piezoelectric ceramics with high hydrostatic figure of merits using camphene-based freeze casting, *Journal of the American Ceramic Society* 90 (2007) 2807-2813.
- [24] R. Guo, C.-A. Wang, A. Yang, Effects of pore size and orientation on dielectric and piezoelectric properties of 1-3 type porous PZT ceramics, *Journal of the European Ceramic Society* 31(4) (2011) 605-609.
- [25] C.-A.W. Rui Guo, and Ankun Yang, Piezoelectric properties of the 1-3 type porous lead zirconate titanate ceramics, *Journal of the American Ceramic Society* 94(6) (2011) 1794-1799.
- [26] T. Xu, C.-A. Wang, Grain Orientation and Domain Configuration in 3-1 Type Porous PZT Ceramics with Ultrahigh Piezoelectric Properties, *Journal of the American Ceramic Society* 98(9) (2015) 2700-2702.
- [27] Z. Wang, X. Shen, N.M. Han, X. Liu, Y. Wu, W. Ye, J.-K. Kim, Ultralow Electrical Percolation in Graphene Aerogel/Epoxy Composites, *Chemistry of Materials* 28(18) (2016) 6731-6741.
- [28] T. Xu, C.-A. Wang, Effect of two-step sintering on micro-honeycomb BaTiO₃ ceramics prepared by freeze-casting process, *Journal of the European Ceramic Society* 36(10) (2016) 2647-2652.
- [29] C.-A.W. Tingting Xu, Cheng Wang, Synthesis and magnetoelectric effect of composites with CoFe₂O₄-epoxy embedded in 3–1 type porous PZT ceramics, *Ceramics International* 41(9) (2015) 11080-11085.
- [30] S. Zhu, L. Cao, Z. Xiong, C. Lu, Z. Gao, Enhanced piezoelectric properties of 3-1 type porous 0.94Bi_{0.5}Na_{0.5}TiO₃-0.06BaTiO₃ ferroelectric ceramics, *Journal of the European Ceramic Society* 38(4) (2017) 2251-2255.
- [31] Manabu Fukushima, Takahiro Fujiwara, Tobias Fey, K.-i. Kakimoto, One- or two-dimensional channel structures and properties of piezoelectric composites via freeze-casting, *Journal of the American Ceramic Society* 100 (2017) 5400-5408.

- [32] A. Yang, C.A. Wang, R. Guo, Y. Huang, C.W. Nan, Porous PZT ceramics with high hydrostatic figure of merit and low acoustic impedance by TBA-based gel-casting process, *Journal of the American Ceramic Society* 93(5) (2010) 1427-1431.
- [33] A. Yang, C.A. Wang, R. Guo, Y. Huang, C.W. Nan, Effects of sintering behavior on microstructure and piezoelectric properties of porous PZT ceramics, *Ceramics International* 36(2) (2010) 549-554.
- [34] Chunyu Jiang, Xiaoxiao Tian, G. Shi, $K_{0.5}Na_{0.5}NbO_3$ piezoelectric ceramics and its composites fabricated from hydrothermal powders, *Advances in Intelligent Systems Research*, 4th International Conference on Sensors, Mechatronics and Automation (ICSMA 2016), 2016.
- [35] E.P. Gorzkowski, M.J. Pan, Barium titanate-polymer composites produced via directional freezing, *IEEE Transactions on Ultrasonics, Ferroelectrics, and Frequency Control* 56(8) (2009) 1613-1616.
- [36] Q.F. Zhou, B.P. Zhu, C.H. Hu, K.K. Shung, E.P. Gorzkowski, M.J. Pan, Novel piezoelectric ceramic-polymer aligned composites via the freeze casting method for high frequency transducer applications, *Proceedings - IEEE Ultrasonics Symposium*, no. 5441756 2009.
- [37] W. Liu, L. Lv, Y. Li, Y. Wang, J. Wang, C. Xue, Y. Dong, J. Yang, Effects of slurry composition on the properties of 3-1 type porous PZT ceramics prepared by ionotropic gelation, *Ceramics International* 43(8) (2017) 6542-6547.
- [38] G. Liu, T.W. Button, D. Zhang, Lamellar $BaTiO_3$ and its composites fabricated by the freeze casting technique, *Journal of the European Ceramic Society* 34(15) (2014) 4083-4088.
- [39] Y.P. Pin Li, Zijing Dong, Pan Gao, Kaolinite as a suspending agent for preparation of porous $BaTiO_3$ ceramics via freeze casting, *Journal of Electronic Materials* 43(2) (2014) 459-464.
- [40] C.B. Dong Seok Kim, Ho Jin Ma, Do Kyung Kim, Enhanced dielectric permittivity of $BaTiO_3$ /epoxy resin composites by particle alignment, *Ceramics International* 42(6) (2016) 7141-7147.
- [41] G. Benelli, M. Govindarajan, M.S. AlSalhi, S. Devanesan, F. Maggi, High toxicity of camphene and γ -elemene from *Wedelia prostrata* essential oil against larvae of *Spodoptera litura* (Lepidoptera: Noctuidae), *Environmental Science and Pollution Research* (2017).
- [42] A.E.H.K.R. J.D. Cirvello, D.R. Farnell and C. Lindamood, Toxicity and carcinogenicity of t-butyl alcohol in rats and mice following chronic exposure in drinking water, *Toxicology and Industrial Health* 11 (1995) 151-166.
- [43] M.S. T.C. Schmidt, H. Weiß and S.B. Haderlein, Microbial degradation of methyl tert-butyl ether and tert-butyl alcohol in the subsurface, *Journal of Contaminant Hydrology* 70 (2004) 173-203.
- [44] I.I. A Sgambato, B De Paola, G Bianchino, A Boninsegna, A Bergamaschi, A Pietroiusti, and A Cittadini Differential toxic effects of methyl tertiary butyl ether and tert-butanol on rat fibroblasts in vitro *Toxicol Ind Health* March 25 (2009) 141-151.

- [45] H.H.S. Chang, Z. Huang, Laminate composites with enhanced pyroelectric effects for energy harvesting, *Smart Materials and Structures* 19(6) (2010) 065018.
- [46] V.Y. Topolov, A.V. Krivoruchko, C.R. Bowen, A.A. Panich, Hydrostatic Piezoelectric Coefficients of the 2–2 Composite Based on [011]-poled 0.71Pb(Mg_{1/3}Nb_{2/3})O₃-0.29PbTiO₃ Single Crystal, *Ferroelectrics* 400(1) (2010) 410-416.
- [47] J. I. Roscow, Y. Zhang, J. T. Taylor, C. R. Bowen, Porous ferroelectrics for energy harvesting applications, *The European Physical Journal Special Topics*. 224 (2015) 2949-2966.
- [48] Y. Zhang, M. Xie, J. Roscow, Y. Bao, K. Zhou, D. Zhang, C.R. Bowen, Enhanced pyroelectric and piezoelectric properties of PZT with aligned porosity for energy harvesting applications, *Journal of Materials Chemistry A* 5(14) (2017) 6569-6580.
- [49] Y. Zhang, L. Li, B. Shen, J. Zhai, Effect of orthorhombic-tetragonal phase transition on structure and piezoelectric properties of KNN-based lead-free ceramics, *Dalton Transactions* 44(17) (2015) 7797-7802.
- [50] K. Zhou, Y. Zhang, D. Zhang, X. Zhang, Z. Li, G. Liu, W.B. Tim, Porous hydroxyapatite ceramics fabricated by an ice-templating method, *Scripta Materialia* 64(5) (2011) 426-429.
- [51] Y. Zhang, K. Zhou, Y. Bao, D. Zhang, Effects of rheological properties on ice-templated porous hydroxyapatite ceramics, *Materials Science and Engineering: C* 33(11) (2013) 340-346.
- [52] A. Lasalle, C. Guizard, E. Maire, J. Adrien, S. Deville, Particle redistribution and structural defect development during ice templating, *Acta Materialia* 60(11) (2012) 4594-4603.
- [53] T. Moritz, H.-J. Richter, Ice-mould freeze casting of porous ceramic components, *Journal of the European Ceramic Society* 27(16) (2007) 4595-4601.
- [54] S. Deville, E. Saiz, A.P. Tomsia, Ice-templated porous alumina structures, *Acta Materialia* 55(6) (2007) 1965-1974.
- [55] S. Deville, Freeze-casting of Porous Biomaterials: Structure, Properties and Opportunities, *Materials* 3(3) (2010) 1913-1927.
- [56] J. Zou, Y. Zhang, R. Li, Effect of Suspension State on the Pore Structure of Freeze-Cast Ceramics, *International Journal of Applied Ceramic Technology* 8(2) (2011) 482-489.
- [57] C.R. Bowen, S. Buschhorn, V. Adamaki, Manufacture and characterization of conductor-insulator composites based on carbon nanotubes and thermally reduced graphene oxide, *Pure & Applied Chemistr* 86(5) (2014) 765-774.
- [58] H. Bai, Y. Chen, B. Delattre, A.P. Tomsia, R.O. Ritchie, Bioinspired large-scale aligned porous materials assembled with dual temperature gradients, *Science Advances* 1(11) (2015) e1500849.
- [59] K. Nagata, Effects of porosity and grain size on hysteresis loops of piezoelectric ceramics (Pb-La) (Zr-Ti)O₃, *Electrical Engineering in Japan* 100(4) (1980) 1-8.
- [60] J.I. Roscow, R.W.C. Lewis, J. Taylor, C.R. Bowen, Modelling and fabrication of porous sandwich layer barium titanate with improved piezoelectric energy harvesting figures of merit, *Acta Materialia* 128 (2017) 207-217.

- [61] C.R. Bowen, H. Kara, Pore anisotropy in 3–3 piezoelectric composites, *Materials Chemistry and Physics* 75(1–3) (2002) 45-49.
- [62] A.N. Rybyanets, Porous piezoceramics: theory, technology, and properties, *IEEE Transactions on Ultrasonics, Ferroelectrics, and Frequency Control* 58(7) (2011) 1492-1507.
- [63] J. Tan, Z. Li, Microstructures, dielectric and piezoelectric properties of unannealed and annealed porous 0.36BiScO₃-0.64PbTiO₃ ceramics, *Journal of Materials Science* 51(11) (2016) 5092-5103.
- [64] J. I. Roscow, Y. Zhang, M. J. Krašný, R. W. C. Lewis, J. T. Taylor, C. R. Bowen, Freeze cast porous barium titanate for enhanced piezoelectric energy harvesting, *Journal of Physics D: Applied Physics* (2018).
- [65] C.R. Bowen, V.Y. Topolov, Piezoelectric sensitivity of PbTiO₃-based ceramic/polymer composites with 0–3 and 3–3 connectivity, *Acta Materialia* 51(17) (2003) 4965-4976.
- [66] T. Zeng, X.L. Dong, H. Chen, Y.L. Wang, The effects of sintering behavior on piezoelectric properties of porous PZT ceramics for hydrophone application, *Materials Science and Engineering: B* 131(1–3) (2006) 181-185.
- [67] T. Zeng, X. Dong, S. Chen, H. Yang, Processing and piezoelectric properties of porous PZT ceramics, *Ceramics International* 33(3) (2007) 395-399.
- [68] H. Chen, X. Dong, T. Zeng, Z. Zhou, H. Yang, The mechanical and electric properties of infiltrated PZT/polymer composites, *Ceramics International* 33(7) (2007) 1369-1374.
- [69] K.A. Klicker, W.A. Schulze, J.V. Biggers, Piezoelectric Composites with 3–1 Connectivity and a Foamed Polyurethane Matrix, *Journal of the American Ceramic Society* 65(12) (1982) C-208-C-210.
- [70] R.E. Newnham, L.J. Bowen, K.A. Klicker, L.E. Cross, Composite piezoelectric transducers, *Materials & Design* 2(2) (1980) 93-106.
- [71] K.A. Klicker, J.V. Biggers, R.E. Newnham, Composites of PZT and Epoxy for Hydrostatic Transducer Applications, *Journal of the American Ceramic Society* 64(1) (1981) 5-9.
- [72] J. Sun, E.K. Akdoğan, M. Vittadello, A. Safari, Development of novel (2-2) piezoelectric composites by direct-write technique, 2008 17th IEEE International Symposium on the Applications of Ferroelectrics, Santa Re, NM, USA, 2008, pp. 1-2.
- [73] M.S. Mirza, T. Yasin, M. Ikram, S. Khan, M.N. Khan, Dielectric and piezoelectric properties of piezoceramic/polymer 1–3 composites fabricated by a modified align-and-fill technique, *Materials Chemistry and Physics* 149(Supplement C) (2015) 670-677.
- [74] A. Chaipanich, R. Rianyo, R. Potong, P. Penpokai, P. Chindaprasirt, Dielectric and Piezoelectric Properties of 2–2 PZT-Portland Cement Composites, *Integrated Ferroelectrics* 149(1) (2013) 89-94.
- [75] C.R. Bowen, D.P. Almond, Modelling the 'universal' dielectric response in heterogeneous materials using microstructural electrical networks, *Materials Science and Technology* 22(6) (2006) 719-724.
- [76] H.K.B.D.R.U. William David. Kingery, *Introduction to Ceramics*, New York ; London : Wiley-Interscience 1976.